Hindawi
Journal of Nanomaterials
Volume 2023, Article ID 3062788, 13 pages
https://doi.org/10.1155/2023/3062788

Research Article

Ionic Liquid-Intercalated Montmorillonite Interfacial-Reinforced Polymer Composite Scaffold

Dongying Li,[1] Pin Li,[1] Haoyu Wang,[1] Haocheng Du,[1] Lixuan Liu,[2] Bin Li,[1] Yong Xu ,[1] Mengqi Li ,[1] and Yanrong Zhou[1]

[1]*Key Laboratory of Hunan Province for Efficient Power System and Intelligent Manufacturing, College of Mechanical and Energy Engineering, Shaoyang University, Shaoyang 422000, China*
[2]*Department of Otolaryngology, Zhuhai People's Hospital Medical Group, Zhuhai 519000, Guangdong Province, China*

Correspondence should be addressed to Yong Xu; xuyong2927@hnsyu.edu.cn and Mengqi Li; sciencefield@163.com

Received 4 September 2022; Revised 25 November 2022; Accepted 30 November 2022; Published 8 February 2023

Academic Editor: Ibrahim Alarifi

Montmorillonite is often used to enhance the mechanical and biological properties of polymer materials, but the weak interaction between the enhanced phase and the matrix limits the enhancement effect. Herein, ionic liquids were introduced as interfacial compatibilizer to improve the dispersion of the enhanced phase in the matrix and interaction between them, and a composite scaffold with enhanced mechanical properties was prepared by selective laser sintering. Specifically, the positively charged terminations of 1-*n*-butyl-3-methylimidazolium in ionic liquids were anchored to the montmorillonite interlayer domain under electrostatic action. At the same time, the long carbon chain at the other end extends in the opposite direction to increase the layer spacing of the montmorillonite, which provides enough space for the intercalation of the polyetheretherketone molecular chain. First, the blue shift of the diffraction peak in the small-angle X-ray diffraction pattern proves the successful insertion of ionic liquids into the interlayered domain of montmorillonite. In addition, the compression test results show that the compressive strength of the modified composite scaffold was increased by 23%, reaching 31.53 MPa. Besides, the composite scaffold exhibits good biomineralization capacity, which may be attributed to ion modification providing more apatite-shaped nucleation sites. These results suggested that the method of modifying inorganic fillers with ionic liquids to enhance mechanical properties and promote mineralization may be an effective means for bone scaffold modification.

1. Introduction

In recent years, the addition of montmorillonite (MMT) to polymers [1] to improve their mechanical properties [2] has attracted widespread attention [3]. However, the inherent incompatibility between inorganic MMT [4] and organic polymers weakens the interfacial bonding between them [5], resulting in reduced mechanical properties of composite scaffolds filled with high content of MMT [6]. Therefore, it is of great significance to improve the compatibility between MMT and polymer [7]. Researchers are committed to modifying MMT to overcome the incompatibility between it and polymer [8] and further improve the mechanical properties [9]. For example, Mushtaq et al. [10] used hexadecyl trimethyl ammonium chloride to graft modified MMT to improve the hydrophilicity of the polylactic acid fiber scaffold and further improve the mechanical properties. Khosravi and Eslami-Farsani [11] reported that MMT modified with 3-glycidoxypropyltrimethoxysilane became a bridge between unidirectional meta-bit fibers and epoxy composites, thereby enhancing the mechanical properties of composites. However, although these methods provide strategies for enhancing the compatibility of MMT and polymers, they mainly act on the outer surface of MMT. This makes it difficult for polymer molecular chains to intercalate into the MMT interlayer space, which leads to phase separation.

Studies have shown that cation exchange-modified MMT [12] can enhance its compatibility with polymers [13, 14]. Ionic liquid (IL) is a new type of green solvent composed of cations and anions. It has high electrochemical and thermal stability [15] and can realize specific functions through its long carbon chain [16]. Belhocine et al. [17] reported an

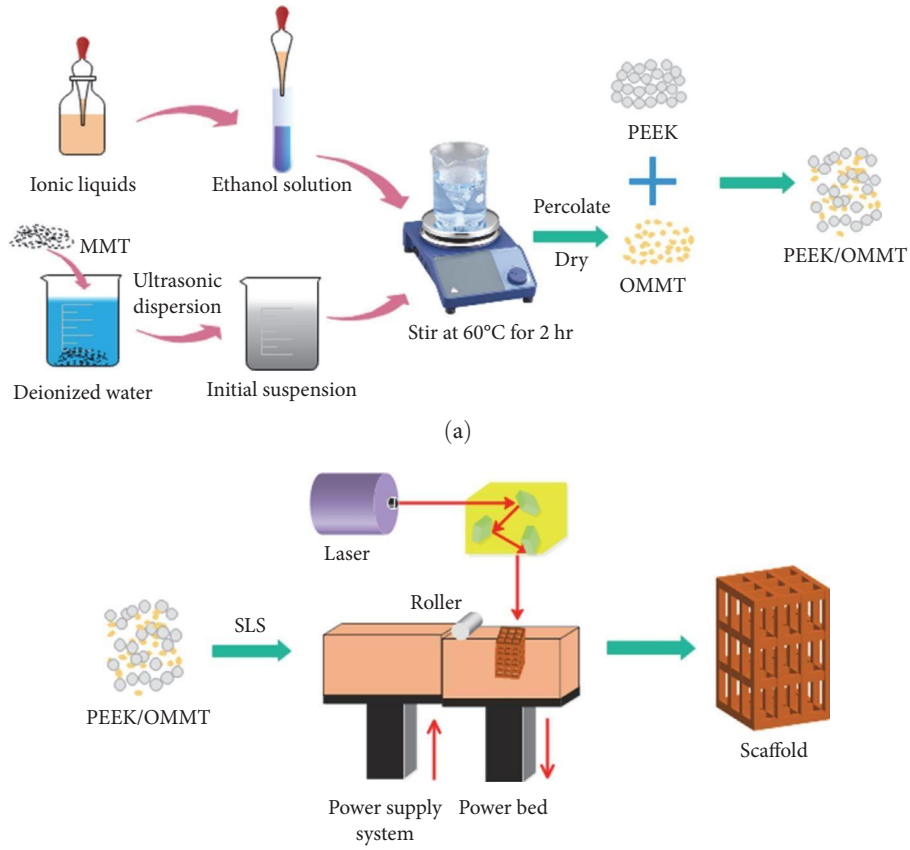

Figure 1: Schematic of the scaffold preparation process: (a) IL organically-modified MMT; (b) preparation of composite scaffold.

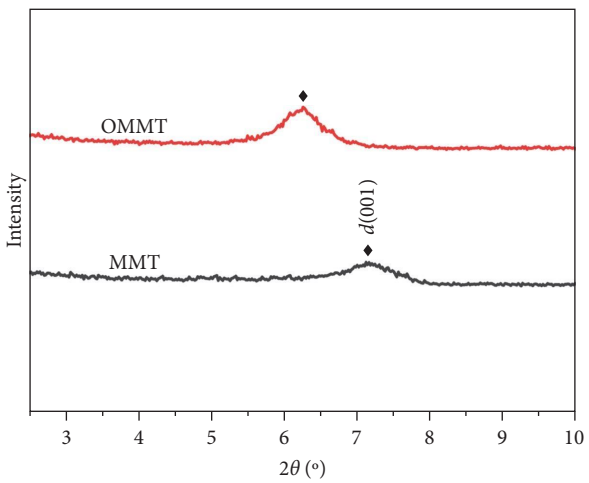

Figure 2: XRD analysis of MMT and OMMT.

increase in the interlayer distance from 11.73 to 15.13 using IL intercalated in MMT, along with a significant enhancement in the crystallinity of the nanomaterials. Therefore, in the process of cation exchange between IL and MMT, the positively charged end of the cation is electrostatically attached to the inner surface of the MMT, and the opposite end containing the long carbon chain stretches to open the interlayer space of the MMT. This facilitates the entry of polymer molecular chain interlayers access to the interlayer space of the MMT. In addition, the polymer molecular chain that completes the intercalation behavior is connected to itself and limited by the force between the parallel layers of MMT. Therefore, under the synergistic effect, the compatibility of MMT and the polymer matrix is significantly enhanced [18], and the uniform dispersion is significantly improved [19].

This article uses polyether ether ketone (PEEK) as the matrix material because of its great biocompatibility and processability [20, 21]. The IL was used to modify MMT to enhance its compatibility with PEEK, and a composite scaffold was prepared by selective laser sintering (SLS). Scanning electron microscopy (SEM) and X-ray diffraction (XRD) were used to characterize MMT's morphological changes and elemental composition changes before and after IL modification. At the same time, the dispersion of MMT in PEEK was evaluated through morphology observation, and the mechanical characteristics of the composite scaffold were assessed through compression experiments. The novelty of this research is firstly the proposal of new materials. The second is the strengthening mechanism of the PEEK molecular chains interspersed into the MMT, which enhances the interfacial bonding. In addition, the degradation performance and biological activity of the scaffold were evaluated in phosphate buffer solution (PBS) and simulated body fluid

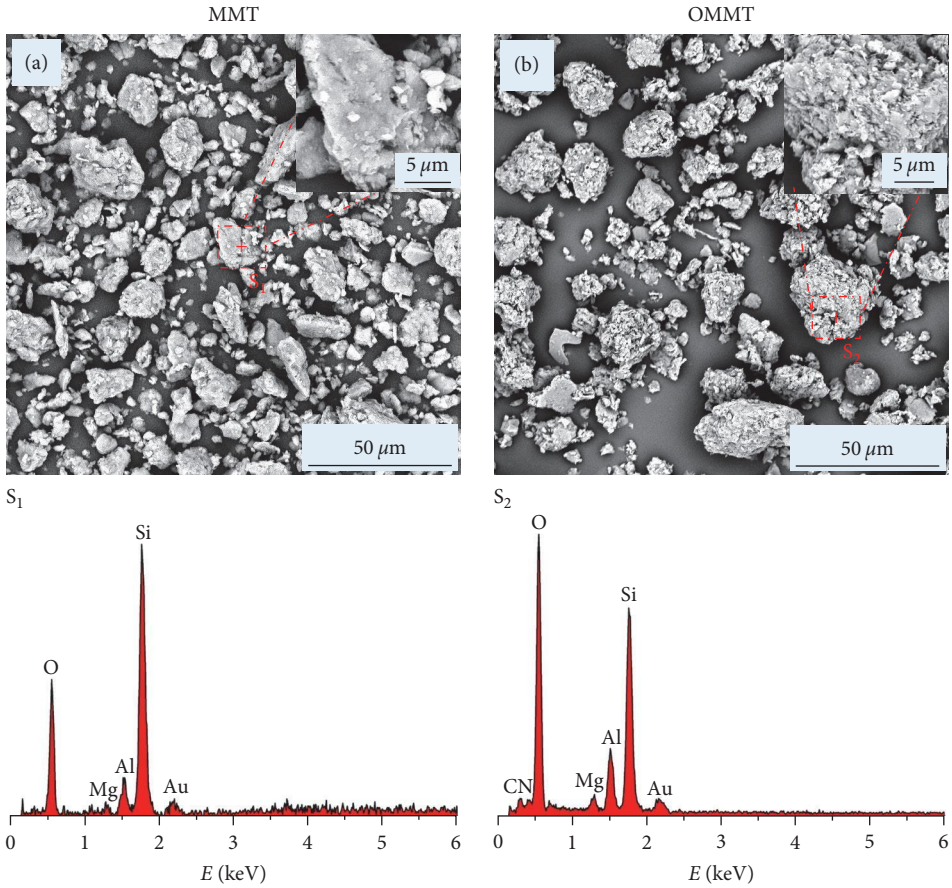

Figure 3: Morphology observation and element analysis of MMT and OMMT. S_1 and S_2 are the EDS spectra of MMT and OMMT, respectively.

Table 1: Element composition of MMT and OMMT.

	O	Si	Al	Mg	C	N
MMT	56.59%	20.60%	2.91%	0.87%		
OMMT	62.05%	13.02%	8.84%	9.12%	3.18%	0.93%

(SBF) immersion experiments and the specific strengthening mechanism of MMT was discussed.

2. Experiment

2.1. Materials. The PEEK powder (purity 99.99%) used in this study was purchased from Guangzhou Yongli New Material Technology Co. Ltd., Guangdong. MMT powder was provided by Beijing Yiwei Special Chemical Manufacturing Co. Ltd. The 1-butyl-3-methylimidazolium hexafluorophosphate was obtained from Shanghai Yuanye Co. Ltd. (CAS No. 17450164-5, purity 99.7%).

2.2. Organic Modification of MMT. Montmorillonite was organically modified with 1-butyl-3-methylimidazolium hexafluorophosphate, as shown in Figure 1(a). First, 5 g of MMT was dispersed in 500 ml of deionized water and stirred for 1 hr at a constant temperature to obtain an initial suspension. Second, 1.5 ml of ionic liquid was dropped into 20 ml of ethanol solution in a 60°C constant-temperature water bath, mixed with the initial suspension of montmorillonite, and then vigorously stirred by a magnetic stirrer for 2 hr. The stirred precipitate was vacuum filtered and rinsed thoroughly with deionized water. Finally, the deposits were placed in a drying oven at 80°C and dried at a constant temperature for 12 hr to obtain modified MMT powder (OMMT).

2.3. Preparation of the Scaffold. MMT and OMMT powders of 2.5, 5, 7.5, and 10 wt% were added to PEEK, respectively. Take the preparation of composite powder of PEEK and 10 wt% OMMT as an example (Figure 1(a)). First, 4.5 g of PEEK and 0.5 g of OMMT were added to a beaker containing deionized water, and then the beaker was placed on magnetic stirring and dispersed uniformly for 2 hr. The powder was dispersed and filtered three times using a centrifuge. Finally, the powder was dried in a drying oven at 60°C for 12 hr

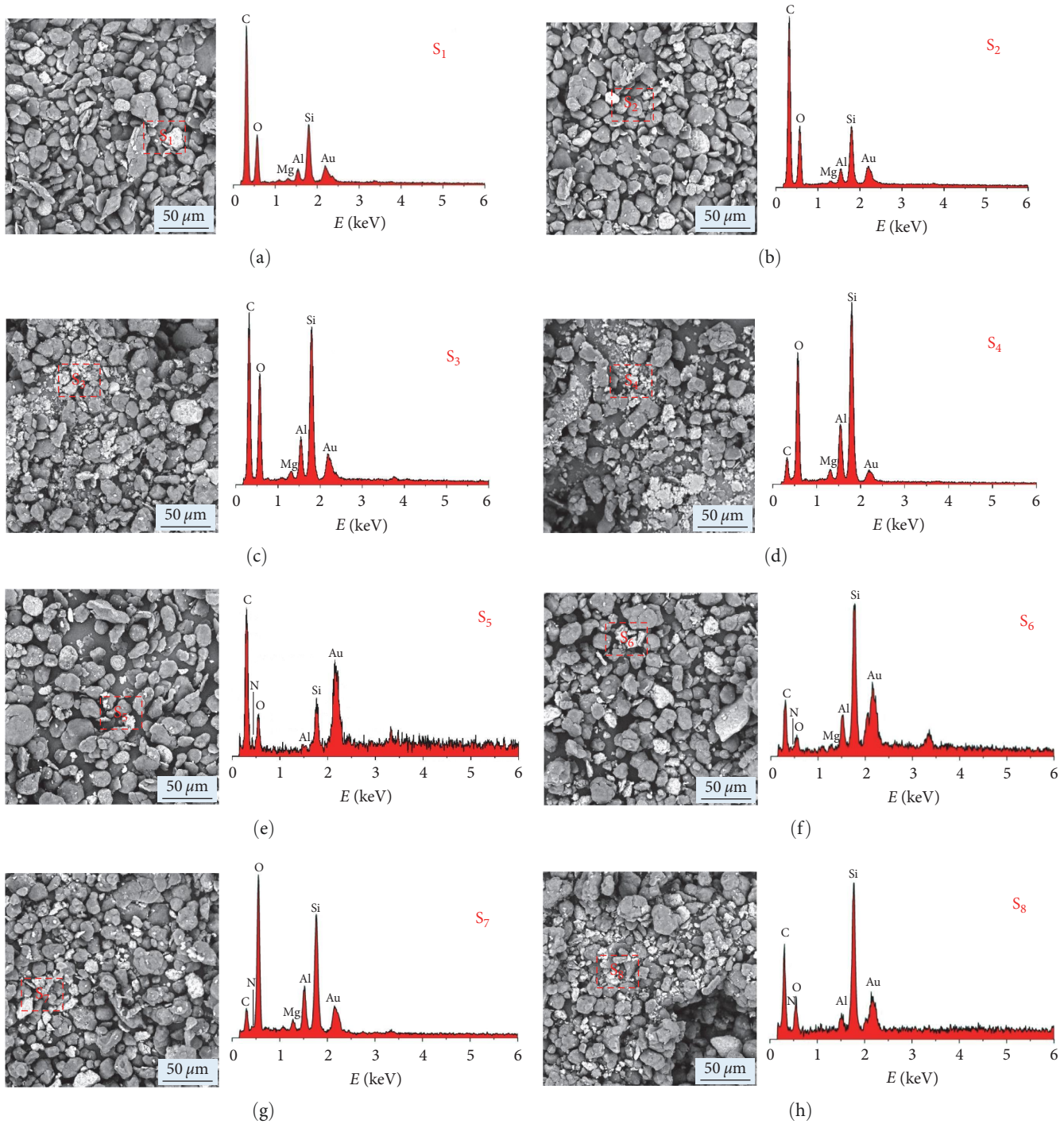

Figure 4: The dispersion of MMT and OMMT in PEEK: (a) PEEK/MMT-2.5 wt%; (b) PEEK/MMT-5 wt%; (c) PEEK/MMT-7.5 wt%; (d) PEEK/MMT-10 wt%; (e) PEEK/OMMT-2.5 wt%; (f) PEEK/OMMT-5 wt%; (g) PEEK/OMMT-7.5 wt%; (h) PEEK/OMMT-10 wt%.

to a constant weight to obtain a composite powder (PEEK/OMMT-10 wt%). The preparation steps of other types of composite powders are similar to those described above.

A self-made SLS system was used to prepare a composite scaffold, as shown in Figure 1(b). First, a model of the porous support ($10 \times 5\ mm^3$) was created using 3D software and exported to .STL format. The .STL file was then sliced to generate the laser-machined object. Finally, the powder was uniformly diffused and shaped by laser sintering with the unsintered powder acting as a powder bed support. The printing process parameters were set as laser power 2.25 W, laser speed 15 mm/s, powder layer thickness 0.1 mm, and scanning interval 1.00 mm.

2.4. Characterization. XRD (AL-2700B, Dandong Aolong Ray Instrument Co. Ltd., China) can be used to analyze

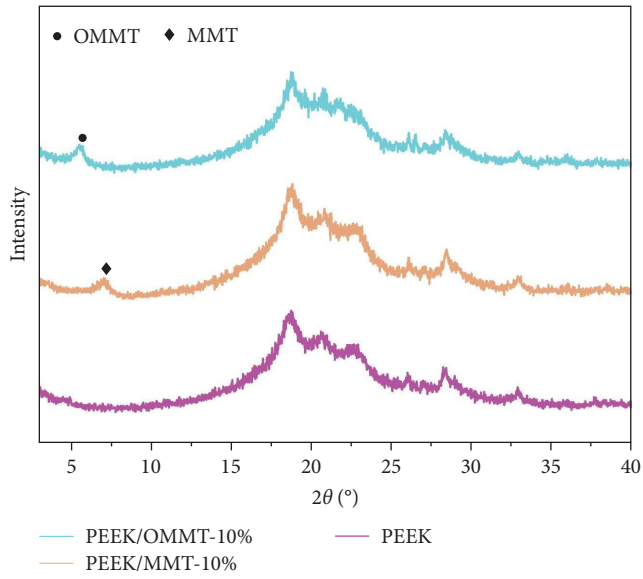

Figure 5: XRD spectra of PEEK, PEEK/MMT-10%, and PEEK/OMMT-10% scaffolds.

the constituent phases of the sample to be measured. Using Cu Kα radiation, the measuring range was 2°–10° and the step angle was 0.02°. The MMT layer spacing was calculated by the Bragg's equation $2d \sin\theta = n\theta$ (d is the crystal plane spacing, θ is the angle between the incident X-rays and the corresponding crystal plane, λ is the wavelength of the X-rays, and η is the number of diffraction levels).

SEM (Finner Science and Technology Co. Ltd., the Netherlands) was used to analyze the surface morphology and dispersion state of the sample. Before the viewing, the sample was plated with gold for 120 s using a sputtering instrument (JS1600, Beijing Hetong Chuangye Technology Co. Ltd., China). An energy dispersive spectrometer (EDS) installed on the SEM was used to perform elemental analysis on the sample to clarify the elemental changes.

2.5. Mechanical Properties. A universal tensile testing machine was used (ZQ-990LA, Dongguan Zhiqu Precision Instrument Co. Ltd., China) to evaluate the compressive strength of the scaffold at a speed of 0.5 mm/min. Each group of samples contains five repeated standard compression parts; the sample size is a cylinder of $\varphi 10 \times 10$, and the average value and deviation are calculated based on the samples.

2.6. Degradability. The samples were immersed in PBS at 37°C and pH = 7.4 for 28 days and the surface morphology was characterized by SEM to evaluate the degradation characteristics. Each group used five sample slices ($\Phi 10 \times 2\,\text{mm}^3$), which were rinsed with ethanol and put into a centrifuge tube containing 20 ml of PBS solution and then sealed and placed in a thermostat. After the predetermined soaking time has arrived, the sample is removed and cleaned with deionized water. Finally, the sample was transferred in a drying oven to dry completely.

2.7. Biomineralization. Samples were immersed in SBF at 37°C for 14 and 28 days, changing the solution every 2 days. After reaching the planned immersion time, the samples were removed from the SBF solution and rinsed three times with deionized water. Finally, the samples were dried in a desiccator for 24 hr before further characterization.

2.8. Statistical Analysis. Test data were solved by one-way analysis of variance and expressed as mean ± standard error. When $P < 0.05$, significant differences were indicated as *.

3. Results and Discussion

3.1. Characterization of MMT and OMMT. XRD is a suitable means to characterize the increase of MMT layer spacing. The XRD diffraction analysis of MMT and OMMT is shown in Figure 2. According to the Bragg's formula, the diffusion peak of MMT appears at $2\theta = 7.15°$, and the corresponding interlayer spacing d (001) = 1.23 nm. However, the diffraction peak of OMMT moves to $2\theta = 6.24°$, corresponding to the interlayer spacing d (001) = 1.44 nm. The left shift of the (001) diffraction peak and the increase in the value represented that the organic cations in IL have exchanged with the cations between MMT layers and were embedded in the interlayer space of MMT, which was same as previous studies [22, 23].

Figure 3 shows the surface morphology of MMT and OMMT. In this case, Figure 3(a) shows pure MMT, which can be seen to have a smooth and flat surface with a distinct layered structure. However, from Figure 3(b), the surface wrinkles of the OMMT have increased significantly, which further indicates that the MMT has been successfully modified [12]. The element composition of MMT and OMMT was analyzed by EDX, as shown in Table 1. The element composition of MMT is O, Si, Al, and Mg, as shown in Figure 3(S_1). OMMT contains O, C, Si, N, Al, and Mg, as shown in Figure 3(S_2). The outcome showed that MMT was completely modified and IL did not cause damage to its components.

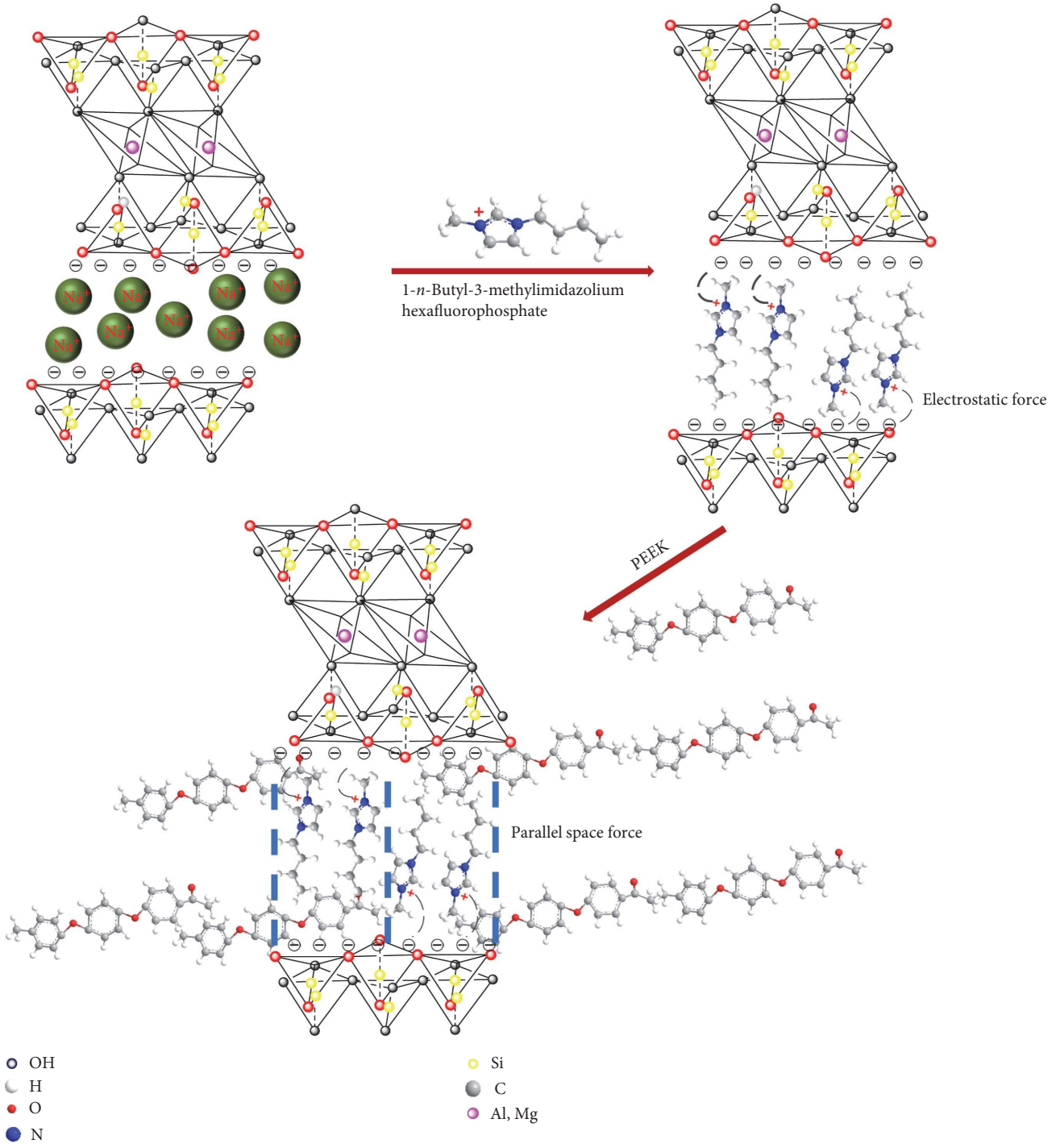

Figure 6: Schematic diagram of modification and intercalation mechanism.

3.2. Characterization of PEEK/MMT and PEEK/OMMT. The dispersion state of MMT and OMMT in the polymer matrix was observed by SEM, as shown in Figure 4. When the contents of MMT and OMMT were 2.5 wt% (Figures 4(a) and 4(e)) and 5 wt% (Figures 4(b) and 4(f)), neither of them showed aggregation in PEEK. However, when the substance of MMT was 7.5 wt% (Figure 4(c)) and 10 wt% (Figure 4(d)), especially when the content was 10 wt%, the obvious agglomeration of MMT can be clearly observed. In contrast, 7.5 wt% (Figure 4(g)) and 10 wt% (Figure 4(h)) of OMMT showed relatively uniform dispersion in PEEK. This may be attributed to the organic modifier promoting the compatibility of MMT and PEEK and enhancing the interface interaction [24, 25]. In addition, the local element composition of PEEK/MMT-2.5, PEEK/MMT-5, PEEK/MMT-7.5, PEEK/MMT-10, PEEK/OMMT-2.5, PEEK/OMMT-5, PEEK/OMMT-7.5, and PEEK/OMMT-10 wt% were analyzed by EDS, as shown in Figure 4 (S_1–S_8).

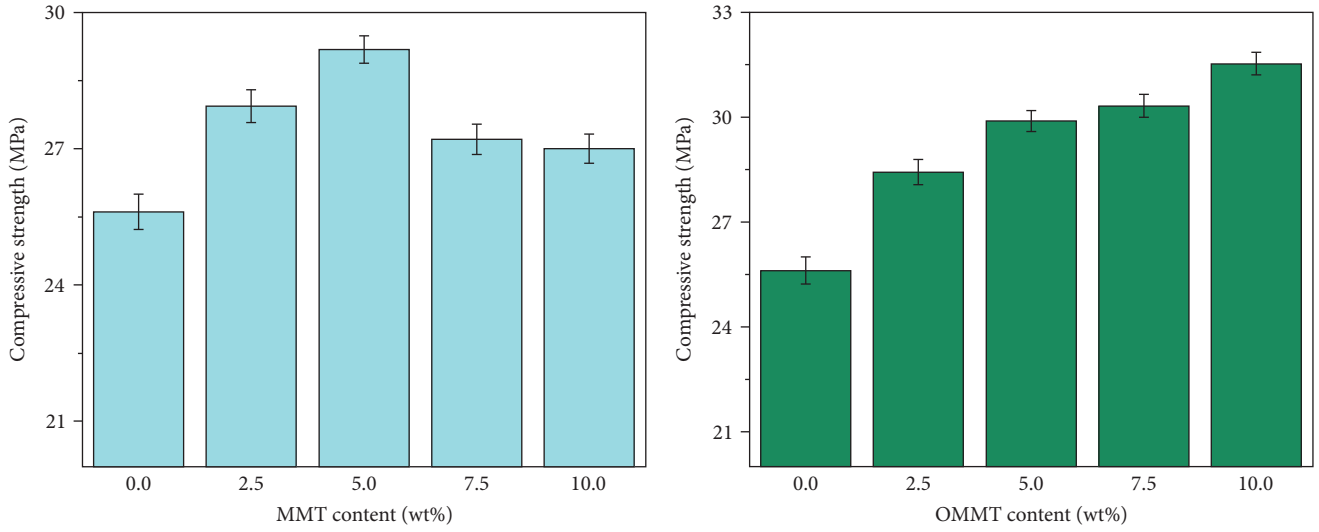

Figure 7: The influence of MMT and OMMT content on the compressive strength of the scaffold: (a) MMT content; (b) OMMT content.

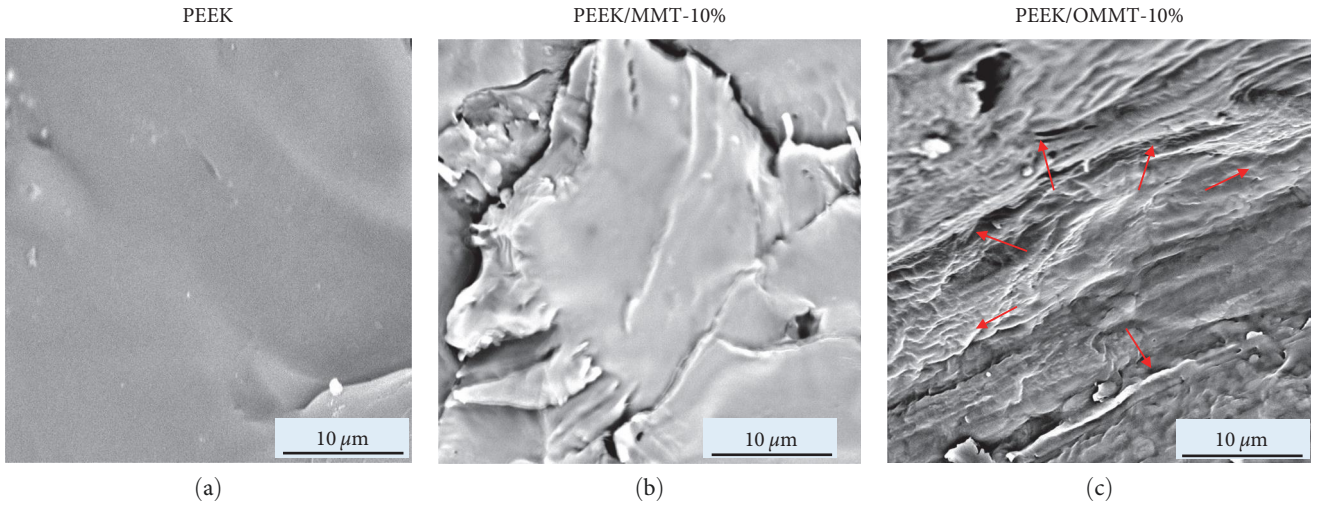

Figure 8: Fracture surface morphology of composite scaffold: (a) PEEK; (b) PEEK/MMT-10 wt%; (c) PEEK/OMMT-10 wt%.

In order to further prove that the PEEK molecular chain intercalates into the space between the layers of MMT, XRD was used to characterize the PEEK, PEEK/MMT-10, and PEEK/OMMT-10 wt% composite scaffolds, as shown in Figure 5. Among them, the pure PEEK scaffold has no peaks in the region of $2\theta = 2°–10°$, and its characteristic peaks were located at $2\theta = 18.8°$, 20.7°, 22.9°, and 28.9° [26]. It can be observed that the characteristic peak of PEEK/MMT-10% at 2°–10° was not significantly different from that of MMT (Figure 2(a)). The constant value of d (001) indicates that the PEEK molecular chain cannot penetrate the interlayer space of the MMT, thus forming an immiscible state. It is worth noting that PEEK/OMMT-10% has a peak shift to the left compared with the (001) characteristic peak in OMMT, as shown in Figure 2(a), which indicates that the OMMT interlayer domain is enlarged, which may be attributed to the PEEK molecule chain intercalation.

3.3. Mechanism Analysis. The mechanism of cationic-modified MMT and PEEK molecular chain intercalation into the interlayer space of MMT was analyzed, as shown in Figure 6. Specifically, after ion exchange between 1-*n*-butyl-3-methylimidazolium and the cations in MMT, its positively charged end was drawn to the negatively charged surface of MMT, resulting in an electrostatic effect. The other end of 1-*n*-butyl-3-methylimidazolium containing a long carbon chain extends in the contrary direction, widening the interlayer spacing of montmorillonite. When the interlayer space of MMT is increased, it can promote the insertion of PEEK molecular chains into the interlayer space. In addition, after the PEEK molecular chain completes the intercalation behavior, its movement is restricted. On one hand, the PEEK molecular chains are connected to each other to form a uniform phase. On the other hand, the spatial force of the MMT parallel layer and the van der Waals force of the modifier increase the difficulty of the movement of the PEEK

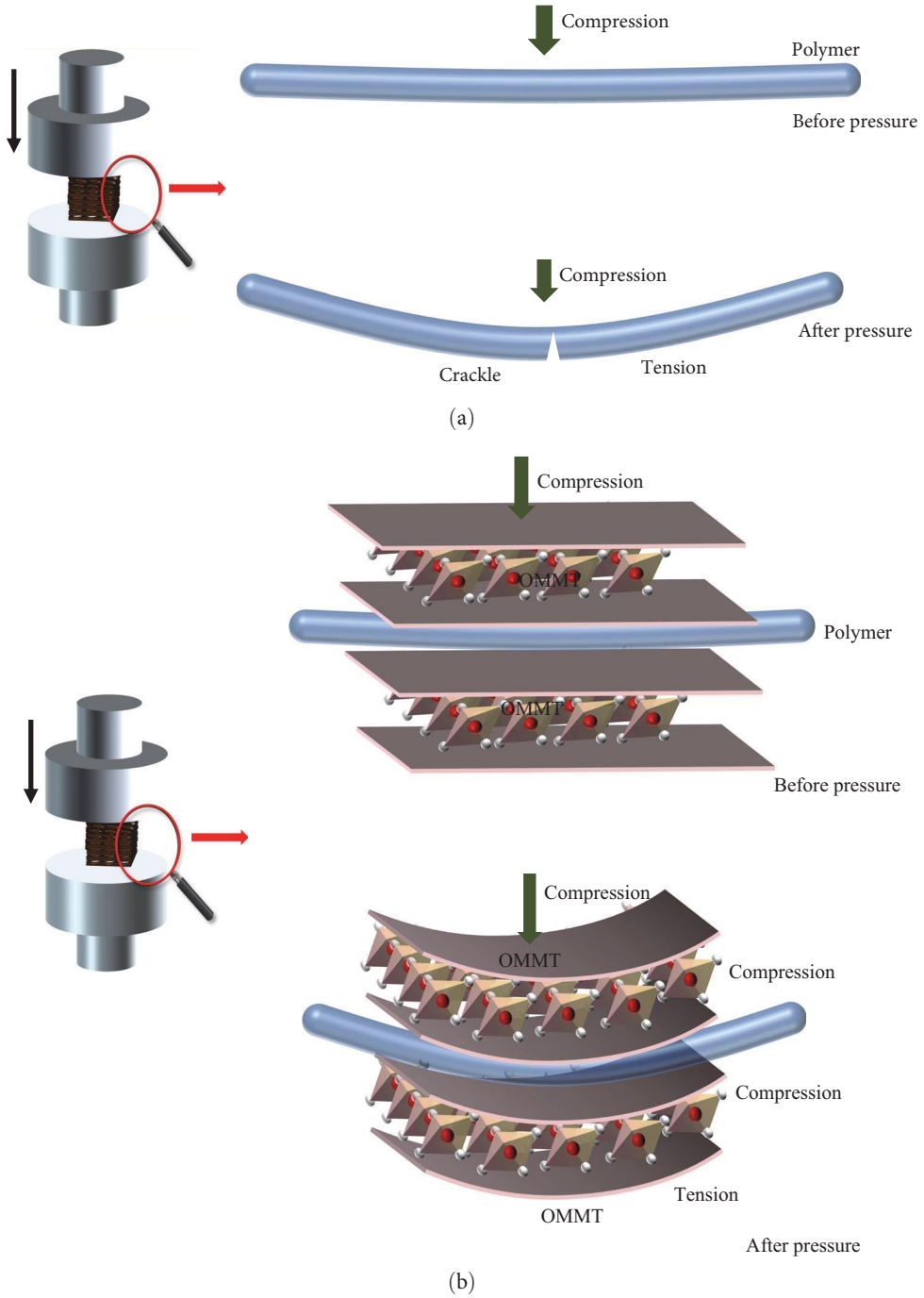

Figure 9: Mechanism analysis of mechanical properties enhancement: (a) the force analysis of PEEK molecular chain; (b) analysis of the stress after PEEK is inserted into the interlayer space of OMMT.

molecular chain. In conclusion, IL acts as a compatibilizer, which improves the compatibility of MMT with PEEK and allows PEEK to intercalate MMT more easily, which is expected to have a positive influence on the mechanical properties of the composite scaffolds.

3.4. Mechanical Property. Assessing the compressive strength of composite supports, as shown in Figure 7, in composite scaffolds, inorganic fillers can usually act as load distributors to enhance their compressive performance [27]. When the details of MMT increased from 0 to 10 wt%, the compressive strength of the composite scaffold showed a trend of continuous increase followed by a gradual decrease. This may be attributable to the agglomeration of excessive MMT, which leads to a decrease in the enhancement effect. However, the compressive strength of the scaffold increases with the increase of OMMT content. When its content was 10 wt%, the scaffold exhibits the highest compressive strength (31.53 MPa). This may be attributable to the fact that the modifier improves the compatibility of MMT and polymer

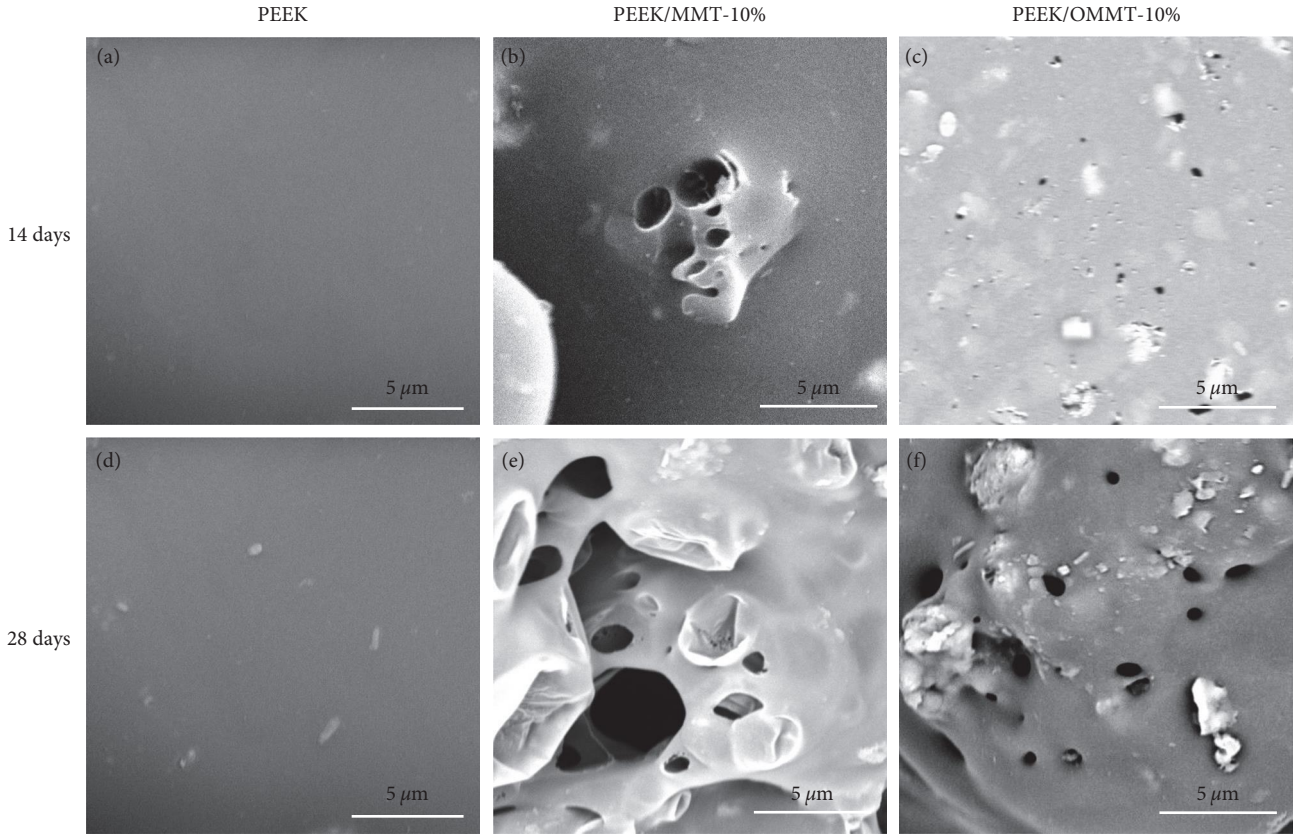

Figure 10: (a, d) PEEK, (b, e) PEEK/MMT-10%, and (c, f) PEEK/OMMT-10% scaffolds are surface morphologies immersed in PBS solution. In (a–c), scaffolds are immersed for 14 days and in (d–f), for 28 days.

and enhances the interface bonding between composite materials. It is well known that uniformly dispersed filler particles have a positive effect on improving the mechanical properties of composite materials. Grigora et al. [28] tested 3D-printed PLA/MMT specimens, which exhibited enhanced mechanical properties. PLA/MMT nanocomposite filaments showed better mechanical properties when using a 4 wt% concentration of MMT. In this experiment, the scaffold with an OMMT content of 10 wt% has the highest compressive strength. Therefore, PEEK/OMMT-10 wt% composite scaffold was selected for subsequent experiments.

3.5. Characterization of a Fracture Surface of Scaffolds. The fracture surface morphologies of PEEK, PEEK/MMT-10 wt%, and PEEK/OMMT-10 wt% were observed by SEM, as shown in Figure 8. Among them, the cross section of the pure PEEK scaffold was smooth and flat, basically without wrinkles (Figure 8(a)). The fracture surface of PEEK/MMT-10 wt% showed a large number of gathered folds (Figure 8(b)), which may be due to the lack of good compatibility and interfacial bonding between the two, which makes PEEK unable to intercalate the interlayer domains of MMT. It is worth noting that the wrinkles of the fracture surface of the PEEK/OMMT-10 wt% composite scaffold were more uniform and finer (Figure 8(c)), which may be attributed to the change in the force on PEEK molecular chains after intercalation of OMMT. This further proves that OMMT has better compatibility and stronger interface bonding with PEEK, which is consistent with the results of the compression experiment.

3.6. Mechanical Property Enhancement Mechanism Diagram. The mechanism by which OMMT enhances the mechanical properties of PEEK was analyzed, as shown in Figure 9. When the PEEK molecular chain is not inserted into the interlayer space of OMMT (Figure 9(a)), it is deformed under the action of pressure, the upper part is under pressure, and tension is formed at the bottom, and the appearance of tension makes the bottom part more prone to cracks. However, when the PEEK molecular chain enters the interlaminar space of the OMMT (Figure 9(b)), its interlaminar structure has a protective effect on the PEEK molecular chain. In detail, the bottom of the OMMT can effectively carry and transfer the tension of the PEEK molecular chain, thereby delaying or avoiding the breaking of the molecular chain. These behaviors promoted the effective enhancement of the mechanical properties of the composite scaffold.

3.7. Degradation Property. The degradation characteristics of PEEK, PEEK/MMT-10, and PEEK/OMMT-10 wt% were evaluated by the change of surface topography, as shown in Figure 10. It can be seen that even after soaking for 14 days (Figure 10(a)) or 28 days (Figure 10(d)), the surface of the PEEK scaffold in the control group was smooth and flat without any holes and gaps, which indicated that PEEK hardly degraded. However, after the addition of PEEK to

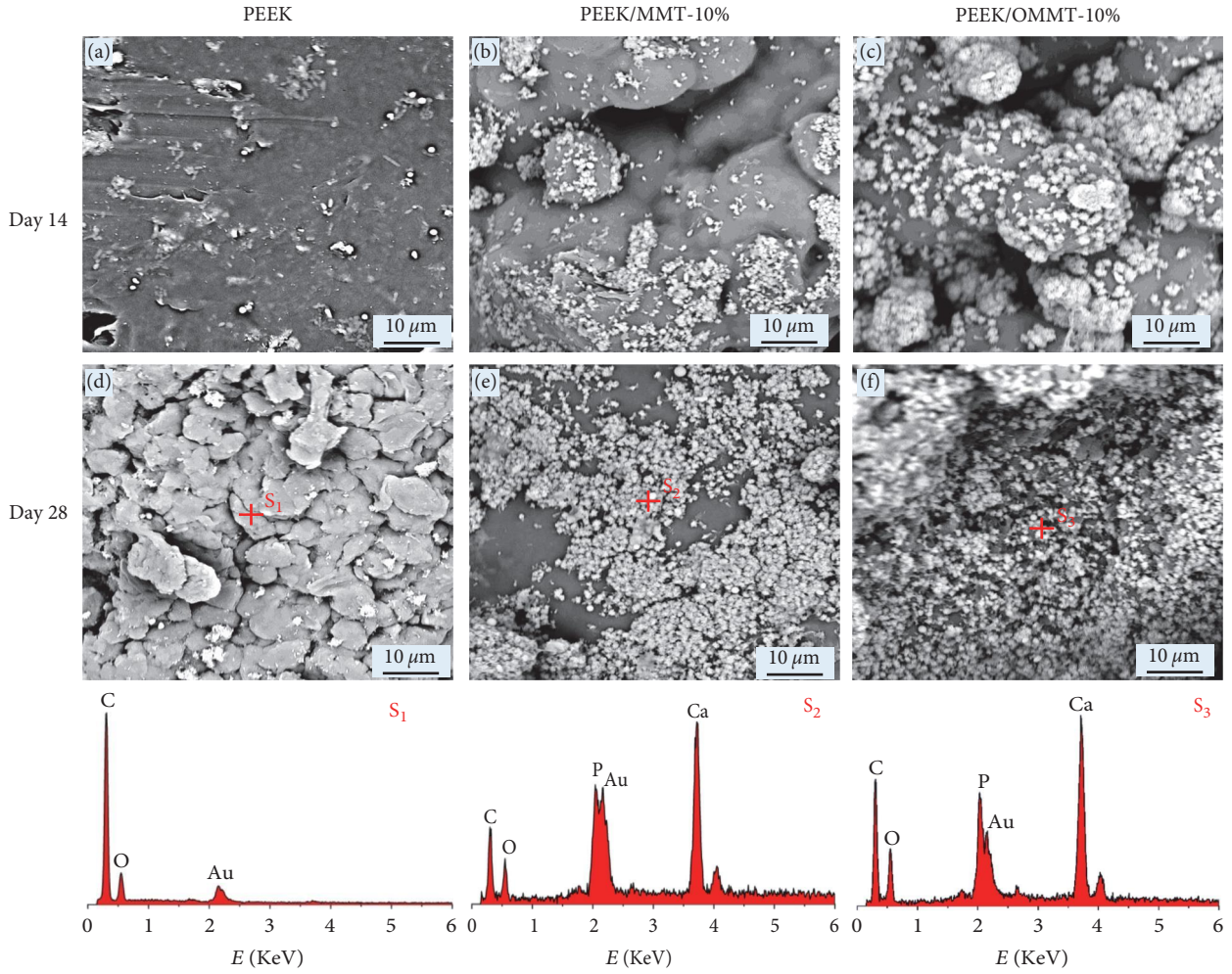

FIGURE 11: (a, d) PEEK, (b, e) PEEK/MMT-10%, and (c, f) PEEK/OMMT-10% scaffolds are surface morphologies immersed in SBF solution. In (a–c), scaffolds are immersed for 14 days and in (d–f), for 28 days. S_1, S_2, and S_3 were EDS spectra of PEEK, PEEK/MMT-10 wt%, and PEEK/OMMT-10 wt% immersed in SBF solution for 28 days, respectively.

MMT and OMMT, the surface morphology of the immersed scaffolds began to change. After soaking for 14 days, fewer aggregated holes and gaps appeared in the PEEK/MMT-10 wt% scaffold, as shown in Figure 10(b). However, after soaking for 28 days (Figure 10(e)), the aggregated pores of PEEK/MMT-10 wt% scaffolds increased. It is worth noting that the PEEK/OMMT-10 wt% scaffolds appeared to show uniform pore size and distribution morphology. Similarly, compared with the scaffold soaked for 14 days (Figure 10(c)), the pores of the scaffold soaked for 28 days were significantly larger (Figure 10(f)). Shuai et al. [29] inserted carbon nanotubes (CNT) into the interlayer of MMT by ionic reaction, improving the hydrophilicity and faster degradability of the scaffold. As we all know, MMT is hydrophilic, which can improve the water absorption capacity of polymer stents, and the enhancement of water absorption performance contributes to the degradation of PEEK scaffold.

3.8. The Ability of Biological Mineralization. Apatite is the main component of human bone, and therefore, the growth of apatite on the scaffold is one of the signs that prove its biological activity [30]. The mineralization abilities of PEEK, PEEK/MMT-10 wt% and PEEK/OMMT-10 wt% scaffolds immersed in SBF for 2 and 4 weeks were evaluated, respectively, as shown in Figure 11. It can be observed that whether it is immersed for 14 days (Figure 11(a)) or 28 days (Figure 11(d)), the PEEK scaffold shows no apatite formation and growth, and only C and O elements are detected in the EDS spectrum (Figure 11(S_1)). In contrast, PEEK/MMT-10 wt% and PEEK/OMMT-10 wt% composite scaffolds both grew apatite after soaking for the same time. Correspondingly, Ca and P elements were detected in their EDS energy spectrum, which further proved the deposition of apatite (Figures 11(S_2) and 11(S_3)). At the same time, the density of apatite after 28 days of immersion was greater than that of the same proportion of stents after 14 days of immersion. In addition, whether it was immersed for 14 days (Figure 11(b)) or 28 days (Figure 11(e)), the apatite growth on the PEEK/MMT-10 wt% scaffold appeared aggregated. After the PEEK/OMMT-10 wt% composite scaffold was soaked for 14 days (Figure 11(c)) and 28 days (Figure 11(f)), especially after 28 days, dense apatite covered the surface of the scaffold, forming a thick apatite layer. In vitro mineralization experiments showed

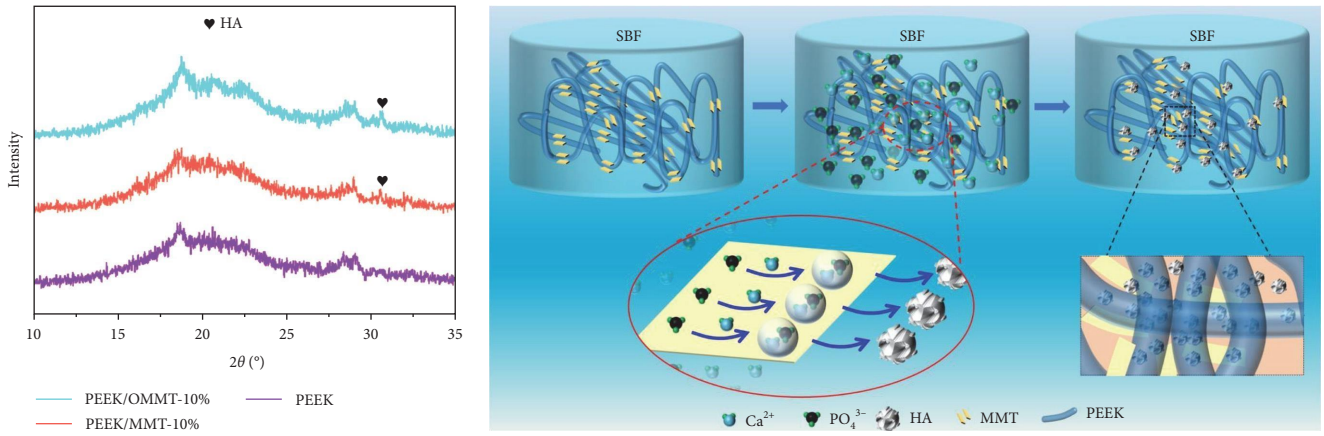

(a) (b)

FIGURE 12: Analysis of the biomineralization mechanism of the composite scaffold: (a) XRD spectra of PEEK, PEEK/MMT-10 wt%, and PEEK/OMMT-10 wt% scaffolds after mineralization; (b) the mechanism of mineralization of OMMT reinforced composite scaffold.

that the modified MMT can increase the biological activity of polymerization, which was consistent with the previous results [31].

Apatite deposition on the composite scaffold was further confirmed by XRD, as shown in Figure 12(a). Compared with pure PEEK scaffolds, apatite characteristic peaks were detected on both PEEK/MMT-10 wt% and PEEK/OMMT-10 wt% composite scaffolds ($2\theta = 30.4°$). It is worth noting that the characteristic peak of apatite on the PEEK/OMMT-10 wt% scaffold is higher, which further shows that OMMT enhances the in vitro mineralization ability of the composite scaffold.

The in vitro mineralization mechanism of PEEK enhanced by OMMT is summarized, as shown in Figure 12(b). The electrostatic effect of MMT was enhanced after cationic modification, resulting in its ability to adsorb ions [32]. Therefore, the introduction of 1-*n*-butyl-3-methylimidazolium in IL has a positive impact on the biomineralization ability of the composite scaffold. In this experiment, the increase in mineralization capacity of the scaffold in vitro is mainly attributed to two aspects. On one hand, the exchange of cations between the cations in IL and MMT layers increases the interlayer spacing, which greatly increases the adsorption capacity of MMT [33]. On the other hand, IL changed the electrostatic effect of MMT, which increased its adsorption capacity for PO_4^{3-}, CO_3^{2-}, and OH^- in SBF solution, providing more nucleation sites for apatite deposition [34]. Therefore, increased adsorption capacity and a large number of nucleation sites promote the formation of apatite.

4. Conclusion

In this study, modified MMT-reinforced PEEK scaffolds were prepared by SLS technique. Among them, ionic liquids as a modification medium successfully expanded the interlayer domain of MMT and ensured the successful intercalation of PEEK molecular chains. Moreover, the modified MMT showed good dispersibility in the PEEK matrix, and significantly improved the mechanical properties of the composite scaffold (reaching 31.53 MPa). In addition, the modified scaffold also has good biomineralization ability. Therefore, the method of ionic liquid-modified inorganic packing to improve mechanical properties and promote mineralization has certain application prospects in bone tissue engineering. The biocompatibility and bioactivity of PEEK/OMMT composite scaffolds in vivo need to be further studied.

Data Availability

The data used to support the findings of this study are included within the article.

Conflicts of Interest

The authors declare that they have no conflicts of interest.

Authors' Contributions

Dongying Li and Pin Li contributed equally to this work.

Acknowledgments

This work was supported by the following funds: (1) Hunan Provincial Natural Science Foundation of China (2021JJ30632, 2020JJ4556, 2022JJ50182); (2) Scientific Research Fund of Hunan Provincial Education Department (21B0686, 18A384, 19K083); Project of Science and Technology Bureau of Shaoyang (2021GZ041); Shaoyang University Graduate Education and Teaching Reform Research Project; Graduate Research and Innovation Project of Shaoyang College (CX2022SY003).

References

[1] P. Arabkhani, A. Asfaram, and M. Ateia, "Easy-to-prepare graphene oxide/sodium montmorillonite polymer nanocomposite with enhanced adsorption performance," *Journal of Water Process Engineering*, vol. 38, Article ID 101651, 2020.

[2] A. H. Bhat, T. A. Rangreez, Inamuddin, and H.-T.-N. Chisti, "Wastewater treatment and biomedical applications of montmorillonite based nanocomposites: a review," *Current Analytical Chemistry*, vol. 18, no. 3, pp. 269–287, 2022.

[3] Z. Wang, H. Sheng, L. Xiang et al., "Different performance of pyrene biodegradation on metal-modified montmorillonite: role of surface metal ions from a bioelectrochemical perspective," *Science of the Total Environment*, vol. 805, Article ID 150324, 2022.

[4] D. S. Dlamini, J. Li, and B. B. Mamba, "Critical review of montmorillonite/polymer mixed-matrix filtration membranes: possibilities and challenges," *Applied Clay Science*, vol. 168, pp. 21–30, 2019.

[5] F. Guo, S. Aryana, Y. Han, and Y. Jiao, "A review of the synthesis and applications of polymer-nanoclay composites," *Applied Sciences*, vol. 8, no. 9, Article ID 1696, 2018.

[6] D. Y. Li, P. Li, Y. Xu et al., "Progress in montmorillonite functionalized artificial bone scaffolds: intercalation and interlocking, nanoenhancement, and controlled drug release," *Journal of Nanomaterials*, vol. 2022, Article ID 7900382, 20 pages, 2022.

[7] M. Kotal and A. K. Bhowmick, "Polymer nanocomposites from modified clays: recent advances and challenges," *Progress in Polymer Science*, vol. 51, pp. 127–187, 2015.

[8] M. Raji, M. E. M. Mekhzoum, A. E. K. Qaiss, and R. Bouhfid, "Nanoclay modification and functionalization for nanocomposites development: effect on the structural, morphological, mechanical and rheological properties," in *Nanoclay Reinforced Polymer Composites*, M. Jawaid, A. Qaiss, and R. Bouhfid, Eds., pp. 1–34, Springer, 2016.

[9] B. Biswas, L. N. Warr, E. F. Hilder et al., "Biocompatible functionalisation of nanoclays for improved environmental remediation," *Chemical Society Reviews*, vol. 48, no. 14, pp. 3740–3770, 2019.

[10] M. Mushtaq, M. Wasim, M. A. Naeem et al., "Composite of PLA nanofiber and hexadecyl trimethyl-ammonium chloride-modified montmorillonite clay: fabrication and morphology," *Coatings*, vol. 10, no. 5, Article ID 484, 2020.

[11] H. Khosravi and R. Eslami-Farsani, "Enhanced mechanical properties of unidirectional basalt fiber/epoxy composites using silane-modified Na^+-montmorillonite nanoclay," *Polymer Testing*, vol. 55, pp. 135–142, 2016.

[12] Y. Meng, B. Zhang, J. Su, and J. Han, "Preparation, characterization and properties of montmorillonite modified PTFE/glass fiber composites," *Fibers and Polymers*, vol. 21, pp. 1126–1133, 2020.

[13] B. K. Bozoğlan, O. Duman, and S. Tunç, "Preparation and characterization of thermosensitive chitosan/carboxymethylcellulose/scleroglucan nanocomposite hydrogels," *International Journal of Biological Macromolecules*, vol. 162, pp. 781–797, 2020.

[14] M. Marques Fernandes and B. Baeyens, "Cation exchange and surface complexation of lead on montmorillonite and illite including competitive adsorption effects," *Applied Geochemistry*, vol. 100, pp. 190–202, 2019.

[15] I. A. Lawal and B. Moodley, "Fixed-bed and batch adsorption of pharmaceuticals from aqueous solutions on ionic liquid-modified montmorillonite," *Chemical Engineering & Technology*, vol. 41, no. 5, pp. 983–993, 2018.

[16] F. S. Jahed, M. Galehassadi, and S. Davaran, "A novel 1,2,3-benzotriazolium based ionic liquid monomer for preparation of MMT/poly ionic liquid (PIL) pH-sensitive positive charge nanocomposites," *Journal of Chemical Sciences*, vol. 131, Article ID 18, 2019.

[17] M. Belhocine, A. Ammari, A. Haouzi, F. Dergal, M. Debdab, and H. Belarbi, "Intercalation effect of 1-methyl-3-(4-vinylbenzyl) imidazol-3-ium chloride ionic liquid on Na-exchanged montmorillonite: synthesis, characterizations, and dielectric spectroscopic analysis," *Journal of Physics and Chemistry of Solids*, vol. 169, Article ID 110846, 2022.

[18] F. Zhao, S. Hu, F. Wang, and L. Wang, "A sulfonated PEEK/PCL composite nanofibrous membrane for periosteum tissue engineering application," *Journal of Materials Science*, vol. 54, pp. 12012–12023, 2019.

[19] X. Gu, X. Sun, Y. Sun et al., "Bioinspired modifications of PEEK implants for bone tissue engineering," *Frontiers in Bioengineering and Biotechnology*, vol. 8, Article ID 631616, 2020.

[20] F. Manzoor, A. Golbang, S. Jindal et al., "3D printed PEEK/HA composites for bone tissue engineering applications: effect of material formulation on mechanical performance and bioactive potential," *Journal of the Mechanical Behavior of Biomedical Materials*, vol. 121, Article ID 104601, 2021.

[21] B. I. Oladapo, S. Abolfazl Zahedi, S. O. Ismail et al., "3D printing of PEEK–cHAp scaffold for medical bone implant," *Bio-Design and Manufacturing*, vol. 4, pp. 44–59, 2021.

[22] L. Reinert, K. Batouche, J.-M. Lévêque et al., "Adsorption of imidazolium and pyridinium ionic liquids onto montmorillonite: characterisation and thermodynamic calculations," *Chemical Engineering Journal*, vol. 209, pp. 13–19, 2012.

[23] W. Abdallah and U. Yilmazer, "Novel thermally stable organomontmorillonites from phosphonium and imidazolium surfactants," *Thermochimica Acta*, vol. 525, no. 1-2, pp. 129–140, 2011.

[24] C. Shuai, L. Yu, P. Feng et al., "Organic montmorillonite produced an interlayer locking effect in a polymer scaffold to enhance interfacial bonding," *Materials Chemistry Frontiers*, vol. 4, no. 8, pp. 2398–2408, 2020.

[25] S. Y. Tong, Z. Wang, P. N. Lim, W. Wang, and E. S. Thian, "Uniformly-dispersed nanohydroxapatite-reinforced poly(ε-caprolactone) composite films for tendon tissue engineering application," *Materials Science and Engineering: C*, vol. 70, Part 2, pp. 1149–1155, 2017.

[26] C. Liu, K. W. Chan, J. Shen, C. Z. Liao, K. W. K. Yeung, and S. C. Tjong, "Polyetheretherketone hybrid composites with bioactive nanohydroxyapatite and multiwalled carbon nanotube fillers," *Polymers*, vol. 8, no. 12, Article ID 425, 2016.

[27] N. Johari, M. H. Fathi, and M. A. Golozar, "Fabrication, characterization and evaluation of the mechanical properties of poly (ε-caprolactone)/nano-fluoridated hydroxyapatite scaffold for bone tissue engineering," *Composites Part B: Engineering*, vol. 43, no. 3, pp. 1671–1675, 2012.

[28] M.-E. Grigora, Z. Terzopoulou, K. Tsongas, D. N. Bikiaris, and D. Tzetzis, "Physicochemical characterization and finite element analysis-assisted mechanical behavior of polylactic acid-montmorillonite 3D printed nanocomposites," *Nanomaterials*, vol. 12, no. 15, Article ID 2641, 2022.

[29] C. Shuai, B. Peng, M. Liu, S. Peng, and P. Feng, "A self-assembled montmorillonite-carbon nanotube hybrid nanoreinforcement for poly-L-lactic acid bone scaffold," *Materials Today Advances*, vol. 11, Article ID 100158, 2021.

[30] A. Olad and F. F. Azhar, "The synergetic effect of bioactive ceramic and nanoclay on the properties of chitosan–gelatin/nanohydroxyapatite–montmorillonite scaffold for bone tissue engineering," *Ceramics International*, vol. 40, Part A, no. 7, pp. 10061–10072, 2014.

[31] L. Yu, Y. Liu, P. Feng, C. Shuai, S. Peng, and A. Min, "Organically modified montmorillonite improves interfacial compatibility between PLLA and PGA in bone scaffold," *Polymer Degradation and Stability*, vol. 182, Article ID 109394, 2020.

[32] I. A. Lawal and B. Moodley, "Fixed-bed and batch adsorption of pharmaceuticals from aqueous solutions on Ionic liquid-modified montmorillonite," *Chemical Engineering & Technology*, vol. 41, no. 5, pp. 983–993, 2018.

[33] M. Zhao, L. Wei, Y. Zheng, M. Liu, J. Wang, and Y. Qiu, "Structural effect of imidazolium-type ionic liquid adsorption to montmorillonite," *Science of The Total Environment*, vol. 666, pp. 858–864, 2019.

[34] L. Wu, Q. Wang, N. Tang, and L. Gao, "Preparation of ionic liquids/montmorillonite composites and its application for diclofenac sodium removal," *Journal of Contaminant Hydrology*, vol. 220, pp. 1–5, 2019.